Erschienen in: Optics letters ; 41 (2016), 16. - S. 3731-3734
https://dx.doi.org/10.1364/OL.41.003731

Stimulated Raman scattering microscopy by Nyquist modulation of a two-branch ultrafast fiber source

Claudius Riek,[1] Claudius Kocher,[1] Peyman Zirak,[2] Christoph Kölbl,[2] Peter Fimpel,[2] Alfred Leitenstorfer,[1] Andreas Zumbusch,[2,*] and Daniele Brida[1]

[1]*Department of Physics and Center for Applied Photonics (CAP), University of Konstanz, D-78457 Konstanz, Germany*
[2]*Department of Chemistry and Center for Applied Photonics (CAP), University of Konstanz, D-78457 Konstanz, Germany*
**Corresponding author: andreas.zumbusch@uni-konstanz.de*

A highly stable setup for stimulated Raman scattering (SRS) microscopy is presented. It is based on a two-branch femtosecond Er:fiber laser operating at a 40 MHz repetition rate. One of the outputs is directly modulated at the Nyquist frequency with an integrated electro-optic modulator (EOM). This compact source combines a jitter-free pulse synchronization with a broad tunability and allows for shot-noise limited SRS detection. The performance of the SRS microscope is illustrated with measurements on samples from material science and cell biology.

Optical microscopy is a key technology for research and diagnosis in a biomedical context. Both the development of efficient labeling methods and the improvements in optical systems have led to impressive progress of fluorescence-based techniques. Yet, these commonly require artificial staining, thus limiting their applicability in many cases. For this reason, the development of label-free microscopy methods has flourished over the last two decades. Among these approaches, nonlinear Raman microscopy has stirred a lot of attention since it promises the generation of specific molecular contrast based on the vibrational spectra of a sample under study. In this regard, nonlinear Raman techniques are especially interesting since they overcome some of the drawbacks of spontaneous Raman microscopy, namely, its slow image acquisition and its susceptibility against the fluorescence background of the sample. The first nonlinear Raman imaging scheme introduced was coherent anti-Stokes Raman scattering (CARS) [1,2]. By tuning the frequency difference of the exciting pump and Stokes laser on resonance with a vibrational transition, significant enhancement of the CARS signal occurs. The implementation of a CARS microscopy experiment is straightforward, since the signal can be separated from the excitation by virtue of an optical filter. This type of microscopy is directly applicable to the investigation of biological tissues where the backscattered CARS light is detected [3]. However, CARS microscopy suffers from the presence of a purely electronic nonresonant background signal, which complicates quantitative interpretation of the data and impedes access to the spectroscopically relevant fingerprint region. These problems can be circumvented by exploiting stimulated Raman scattering (SRS), which is not accompanied by a nonresonant background [4–6]. Also in this case, the frequency difference of a Raman pump and the Stokes beam is tuned to be resonant with a vibrational resonance. In contrast to CARS microscopy, the signal is now detected either as a loss in the intensity of the pump laser or as an energy gain in the Stokes beam. This approach leads to the necessity of detecting small changes in intensity on a very strong background signal, which is usually achieved by employing lock-in detection. This readout technique strongly benefits from the implementation of fast pump modulation with the optimum condition achieved at the Nyquist frequency, i.e., modulation at half of the laser repetition rate.

The specific requirements of SRS microscopy have motivated a number of different laser source developments and experimental geometries. The main criteria to be met are (i) low timing jitter between the two exciting optical pulses, (ii) broadband tunability of the frequency difference between them, and (iii) high-frequency modulation of one of the two pulse trains. With respect to the reduction of timing jitter, designs in which the Stokes and the pump beams are directly generated by a single master source are advantageous. This principle has been applied in the first SRS microscopy experiments in which an ultrafast solid-state laser directly provides the Raman pump while generating the Stokes pulse in a parallel frequency conversion stage, such as an optical parametric amplifier/oscillator or a nonlinear photonic crystal fiber [5–8]. While these systems offer high power and wide-tuning range, they rely on complex nonlinear front ends and display a large footprint. Due to their compactness and stability, fiber lasers have early on been seen as alternatives to large bulk laser systems in nonlinear Raman

microscopy [9,10]. A femtosecond Er:fiber laser system was the first all-fiber source used for SRS microscopy. For this purpose, an Er:fiber oscillator produced seed pulses for two independent Er:fiber amplifiers, the outputs of which were either frequency doubled (Raman pump beam) or sent through a highly nonlinear fiber (HNF) before frequency doubling (Stokes beam) [11]. In a different scheme, the output of an Er:fiber amplifier was sent through an HNF to generate a broadband supercontinuum, which served to seed Tm:fiber or Yb:fiber amplifiers [12,13]. Compared to pure Er:fiber systems, this approach increases the power level of the tunable Stokes but strongly reduces the tuning range.

In all the examples discussed above, modulation of one of the beams driving the SRS process was achieved by exploiting an acusto- or electro-optic modulator (AOM, EOM). This strategy adds complexity and is a potential source of instability to the system. Some recent works included EOMs within the cavity of fiber lasers that had to be electronically synchronized to ancillary sources for the generation of the second pulse train [14,15]. However, femtosecond fiber technology offers a genuine and straightforward possibility for high-frequency modulation since EOMs can be directly integrated before the amplification branches in an all-fiber approach. This scheme features several advantages: (i) in comparison to bulk EOMs operated with driving voltages in the kV range, waveguide-based EOMs with fiber pigtails can be controlled with only 5 V electronics, warranting a high level of stability and reliability; (ii) the EOM is not placed within the oscillator cavity avoiding detrimental feedback effects; and (iii) the modulation frequency can be independent in two distinct amplifiers and may be set to half of the oscillator repetition rate by picking every second pulse. This last aspect is crucial since it guarantees lock-in detection with optimum sensitivity and maximum readout speed.

In this contribution, we report a robust and simple SRS microscope based on a femtosecond Er:fiber system, which makes efficient use of a fiber-integrated EOM for the modulation of the tunable Stokes beam. It combines the advantages of a setup with two independent Er:fiber outputs, namely, broad tunability and inherent jitter-free synchronization of the excitation pulses with the stable modulation up to half of the repetition rate using low-voltage electronics. The noise performance of the setup demonstrates that by the combination of this excitation source with balanced detection, shot-noise limited detection sensitivity can be achieved. The performance of the entire SRS microscope is exemplified by imaging latex beads and human adipocytes.

The experimental setup is depicted in Fig. 1. It consists of a mode-locked Er:fiber oscillator delivering a pulse train at a repetition rate of 40 MHz with a central wavelength of 1562 nm [16]. This emission is split into two replicas, which are used to seed independent broadband Er:fiber amplifiers. In the first arm, the seed light is amplified at the full repetition rate of the oscillator. This stage operates in a regime of nonlinear amplification and generates 300 mW of average power. The pulses are compressed to a temporal duration of approximately 120 fs in an Si prism pair and then frequency doubled in a 10 mm long, periodically poled, $LiNbO_3$ (PPLN) crystal. This branch produces 1.9 nJ pulses (76 mW average optical power) centered at a wavelength of 776 nm, which are employed as Raman pumps in the SRS experiments. The length of the crystal

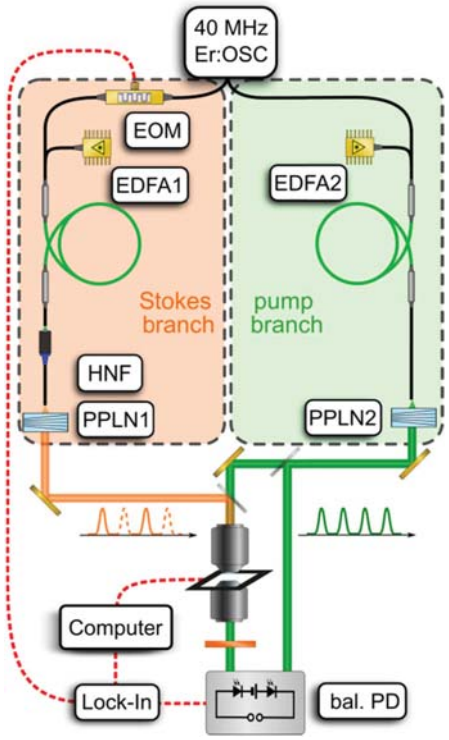

Fig. 1. Schematic layout of the experimental setup. The Er:fiber amplifier that generates the Stokes pulses operates at half of the repetition rate of the oscillator. Er:OSC, Er:fiber oscillator; EOM, electro-optic modulator (AM1550, Jenoptik, Germany); EDFA, Er:doped fiber amplifier; HNF, highly nonlinear fiber; PPLN1/2, periodically poled lithium niobate crystals for second-harmonic generation; and bal. PD, balanced photodetector.

guarantees a spectral bandwidth of the second harmonic (SH) narrower than 1 nm as shown in Fig. 2 (green spectrum at left). The tunable Stokes beam is provided by the second laser branch. In this case, the seed light propagates in a fiber-integrated EOM that is directly spliced after the beam splitter eliminating any free-space propagation. The splitting ratio is 70:30 in favor of the Stokes branch to compensate for the losses introduced by the modulator, thus allowing the amplifier

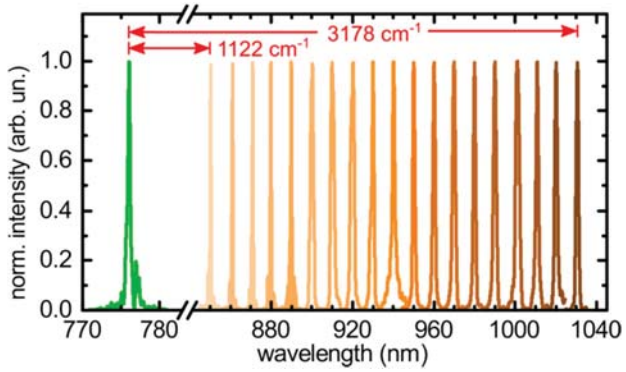

Fig. 2. Series of spectra delivered by the Er:fiber laser system. The green spectrum is the fixed Raman pump while the orange envelopes show the tunability of the Stokes beam. The frequency range that is accessible in SRS experiments spans from 1122 cm^{-1} to 3178 cm^{-1}.

to operate under seeding conditions that are completely analogous to the pump arm. The EOM provides the modulation of the Stokes beam, which allows for the SRS signal detection. Since the lowest noise amplitude and the timing jitter of ultrafast lasers are generally reached at the Nyquist frequency, we inject only every second seed pulse into the subsequent amplifier—equivalent to a trigger for the lock in at 20 MHz modulation. Electronics to control the EOM and for demodulation of the signal are developed in house. The second amplifier is then optimized for operation at half of the repetition rate of the oscillator. After an Si prism compressor, the pulse duration is 120 fs at an average power of 140 mW. The Stokes beam is generated by coupling the output of the 20 MHz amplifier branch into a short HNF for supercontinuum generation. The spectral broadening that occurs in this device produces a dispersive wave that is blueshifted with respect to the fundamental wavelength and a redshifted solitonic component that displays a bandwidth of approximately 500 nm at the central wavelength of 1880 nm. The soliton is first isolated from the rest of the supercontinuum and then focused into a PPLN crystal for SH generation. The nonlinear crystal is engineered with a fan-out design that allows for continuous tuning of the SH wavelength. Up to 10.5 mW of average power at 20 MHz repetition rate is obtained between 850 nm and 1031 nm [16]. Together with the fixed pump wavelength, the vibrational frequencies that can be accessed by the SRS system extend from 1122 cm^{-1} to 3178 cm^{-1}. The complete spectral region of CH- and CD-stretch vibrations and C ≡ C and N ≡ N triple bond stretch vibrations—but also most of the fingerprint regime including the amide bands of proteins—is addressed. The full tuning range of the Stokes is demonstrated by a series of spectra in Fig. 2.

In order to check for the spectral resolution, which can be achieved in coherent Raman experiments, we consider the FWHM of the spectra of pump and Stokes beams that are measured to be 6.1 cm^{-1} and 9.2 cm^{-1}, respectively. The convolution of both envelopes yields a resolution of 12.8 cm^{-1}. As a control, we performed a temporal cross-correlation measurement of the two beams in the focus of the microscope, which yielded an FWHM of 2 ps that can be reconciled with the observed spectral widths. The achieved resolution is ideal for SRS microscopy experiments in a condensed phase where, on the one hand, short pulse durations are necessary for efficiently driving the nonlinear optical process and, on the other hand, typical sample linewidths lie between 10 and 20 cm^{-1}. Note that due to the fact that both pump and Stokes pulses are derived from the same seed source, the experiment has a negligible timing jitter [17] and no active synchronization of the two pulse trains is necessary.

For the stimulated Raman loss microscopy experiments, we overlapped pump and Stokes beams in space and time before coupling them into a homebuilt sample scanning microscope using either a 40×, 0.85 NA air or a 63×, 1.2 NA water immersion objective (Leica, Germany). The transmitted light was collected using a 0.9 NA air or a 1.4 NA oil condenser (Leica, Germany). Modulation at the Nyquist frequency allows access to the frequency at which the Er:fiber laser system has its lowest noise. To further improve the sensitivity to the shot-noise limit, we employed a balanced detection scheme [11] in which a small part of the pump beam bypasses the microscope and is used as a reference on a balanced photodetector (PDB450A, Thorlabs, USA). The transmitted signal was spectrally filtered such that only pump light reached the detector. Using this scheme, we characterized the sensitivity of our experiment (Fig. 3).

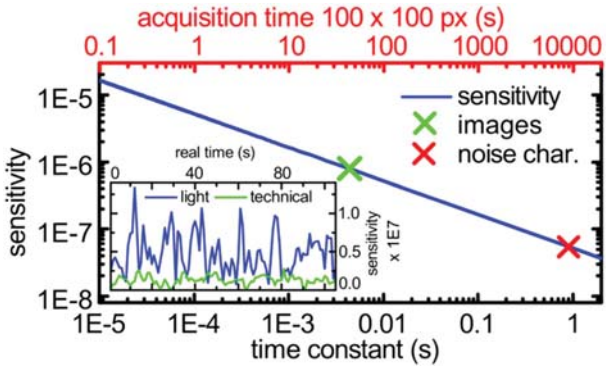

Fig. 3. Sensitivity level (blue line) as the function of time constant and acquisition time for a 100 × 100 pixel image. Two crosses point to the positions for the image acquisition (green) and the noise characterization (red). Inset: noise performance of the system photodetection. The measurement with a 1 Hz lock-in amplifier bandwidth is performed for the 10 mW (blue line in the inset) pump beam intensity on the photodetector. The green line in the inset is the electronic background noise.

The noise performance of the system is influenced by the technical noise level of the detector and the shot noise of the detected pump beam. Both are characterized by analysis of the high-frequency lock-in (HF2, Zurich Instruments, Switzerland) signal for a time constant of $\tau = 0.95$ s. The measurements are depicted in the inset of Fig. 3 and show the demodulated signal over real time. The technical dark noise is estimated by blocking the pump and Stokes beams with no photons impinging on the detector. This contribution amounts to $1.5 \times 10^{-8}/\sqrt{\text{Hz}}$ and is depicted with a green line. With the full pump beam impinging on the balanced photodetector, the minimal noise level for the optical signal is observed as the blue line at $5.4 \times 10^{-8}/\sqrt{\text{Hz}}$. The noise measurement defines the sensitivity for the detected SRS signal, which is very close to the shot-noise level and thereby to the ultimate limit for this approach. Based on the time constant of the lock-in amplifier, the acquisition time for a 100 × 100 pixel image can be calculated. Spending less time per pixel lowers the sensitivity but speeds up the acquisition time. The main panel of Fig. 3 quantifies this dependence. By accepting a lower signal-to-noise level, the acquisition of the images can be accelerated to below 1 s, thus opening the way to video rate SRS microscopy. Remarkably, at a 10 Hz frame rate, the sensitivity would still reach a level as low as 1.8×10^{-5}.

In order to demonstrate the imaging performance of our experimental setup, we recorded scans of different test samples (Fig. 4). The spectral resolution was checked by imaging a mixture of polymethyl methacrylate (PMMA) and polystyrene (PS) beads on a microscope slide. The left part of Fig. 4 was recorded at a wavenumber difference between pump and Stokes of $\Delta\nu = 3053$ cm^{-1}, whereas the image to the right was taken at $\Delta\nu = 2946$ cm^{-1}. The experimental results show that both compounds can clearly be distinguished on the basis of their vibrational resonances. In fact, whereas PMMA only contains aliphatic CH with vibrational resonances for the stretch

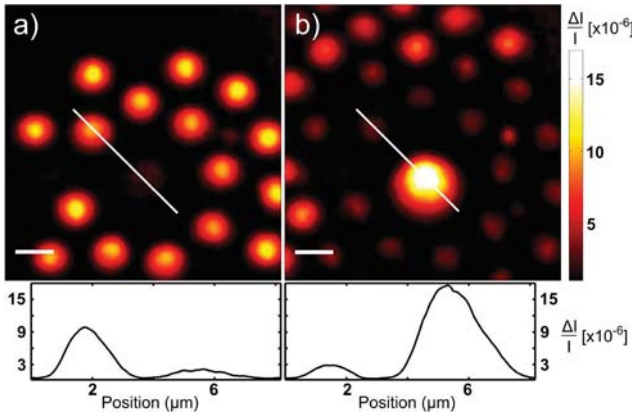

Fig. 4. Stimulated Raman loss microscopy of a mixture of PMMA (1 to 10 μm diameter) and PS beads (3 μm diameter). The images were recorded at Raman shifts of (a) 3053 cm^{-1} corresponding to the aromatic CH resonance in PS and of (b) 2946 cm^{-1} corresponding to the aliphatic CH resonance in PMMA, respectively. The excitation intensities were 3.9 mW at 776 nm (pump beam) and 1.5 mW at 1006 nm or 1.2 mW at 1017 nm (Stokes beams). The pixel dwell times were 5 ms. Lower panels: section of the images at the position indicated in the upper panel with a solid white line. Size bar: 2 μm.

vibrations below 3000 cm^{-1}, PS additionally contains aromatic CH with resonances at ~3050 cm^{-1}. The remaining contrast is due to the finite spectral overlap of the vibrational bands of PS and PMMA. The lower panels in Fig. 4 include a section of the images to prove the diffraction-limited spatial resolution achieved at the focus of the beams.

As a final proof-of-principle experiment, we employed the setup for imaging of a biological sample, namely, fixed human 3T3 cells (Fig. 5). They were imaged at a Raman resonance frequency of $\Delta\nu = 2823$ cm^{-1}, which corresponds to the vibrational excitation of aliphatic CH present in the lipid droplets contained in the cytoplasm. One should note that for recording the images the power level at the sample was kept below 10 mW—a value lower than commonly used for nonlinear optical microscopy and compatible with in-vivo experiments. In our case, the imaging speed is limited mainly by the saturation of the photodiode at less than 5 mW. We thus expect

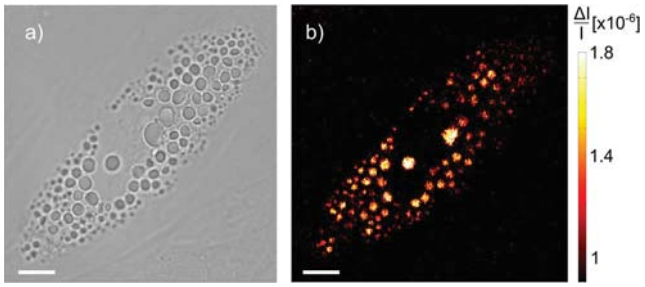

Fig. 5. (a) White-light transmission and (b) stimulated Raman loss microscopy of fixed human adipocytes. The image was recorded at a Raman shift of 2823 cm^{-1} corresponding to an aliphatic CH-stretch vibrational resonance. Lipid droplets containing large amounts of aliphatic CH are visible with high contrast in the SRS image. Excitation powers were as low as 6.5 mW at 776 nm (pump) and 1.8 mW at 994 nm (Stokes). The pixel dwell times were 5 ms. Size bar: 10 μm.

that use of a different detector with a higher saturation level would allow a significant decrease in image acquisition times especially for situations in which optical power on the sample is not of concern.

In conclusion, we describe a novel excitation source for SRS microscopy based on a compact and robust two-branch Er:fiber laser. The fiber-optical integration of the EOM readily allows high-frequency modulation of the output of one of the two branches while maintaining its jitter-free synchronization with the second branch. The frequency difference between the outputs of both branches can be tuned over a very wide spectral range. These features make the system an ideal source for SRS microscopy. Our data show that modulation at the Nyquist frequency together with balanced detection enables SRS microscopy with shot-noise limited detection sensitivity. This is exemplified with high-resolution images of polymer samples as well as of biological cells. The versatility of our setup and its facile adaptability to different experimental conditions let us expect that similar Er:fiber-based systems will increasingly find use in nonlinear optical vibrational microspectroscopy.

Acknowledgment. We thank Martin Winterhalder for scientific discussions, Stefan Eggert for advice on electronics, Britta Kerndl for sample preparation, and Patrick Storz for helping with the laser setup.

REFERENCES

1. M. D. Duncan, J. Reintjes, and T. J. Manuccia, Opt. Lett. **7**, 350 (1982).
2. A. Zumbusch, G. R. Holtom, and X. S. Xie, Phys. Rev. Lett. **82**, 4142 (1999).
3. C. L. Evans, E. O. Potma, M. Puoris'haag, D. Cote, C. P. Lin, and X. S. Xie, Proc. Natl. Acad. Sci. **102**, 16807 (2005).
4. E. Ploetz, S. Laimgruber, S. Berner, W. Zinth, and P. Gilch, Appl. Phys. B **87**, 389 (2007).
5. C. W. Freudiger, W. Min, B. G. Saar, S. Lu, G. R. Holtom, C. W. He, J. C. Tsai, J. X. Kang, and X. S. Xie, Science **322**, 1857 (2008).
6. P. Nandakumar, A. Kovalev, and A. Volkmer, New J. Phys. **11**, 033026 (2009).
7. T. Steinle, V. Kumar, A. Steinmann, M. Marangoni, G. Cerullo, and H. Giessen, Opt. Lett. **40**, 593 (2015).
8. S. Saint-Jalm, P. Berto, L. Jullien, E. R. Andresen, and H. Rigneault, J. Raman Spectrosc. **45**, 515 (2014).
9. G. Krauss, T. Hanke, A. Sell, D. Träutlein, A. Leitenstorfer, R. Selm, M. Winterhalder, and A. Zumbusch, Opt. Lett. **34**, 2847 (2009).
10. M. Marangoni, A. Gambetta, C. Manzoni, V. Kumar, R. Ramponi, and G. Cerullo, Opt. Lett. **34**, 3262 (2009).
11. A. Gambetta, V. Kumar, G. Grancini, D. Polli, R. Ramponi, G. Cerullo, and M. Marangoni, Opt. Lett. **35**, 226 (2010).
12. N. Coluccelli, V. Kumar, M. Cassinerio, G. Galzerano, M. Marangoni, and G. Cerullo, Opt. Lett. **39**, 3090 (2014).
13. C. W. Freudiger, W. L. Yang, G. R. Holtom, N. Peyghambarian, X. S. Xie, and K. Q. Kieu, Nat. Photonics **8**, 153 (2014).
14. Y. Ozeki, Y. Kitagawa, K. Sumimura, N. Nishizawa, W. Umemura, S. Kajiyama, K. Fukui, and K. Itoh, Opt. Express **18**, 13708 (2010).
15. K. Nose, Y. Ozeki, T. Kishi, K. Sumimura, N. Nishizawa, K. Fukui, Y. Kanematsu, and K. Itoh, Opt. Express **20**, 13958 (2012).
16. D. Brida, G. Krauss, A. Sell, and A. Leitenstorfer, Laser Photon. Rev. **8**, 409 (2014).
17. F. Adler, K. Moutzouris, A. Leitenstorfer, H. Schnatz, B. Lipphardt, G. Grosche, and F. Tauser, Opt. Express **12**, 5872 (2004).